Preprint
UCRL-JC-146627-Rev-1

Mapping Phase Transformation in the Heat-Affected-Zone of Carbon Manganese Steel Welds using Spatially Resolved X-Ray Diffraction

J. W. Elmer, J. Wong, T. Ressler, T. A. Palmer

This article was submitted to
6th International Conference on Trends in Welding Research, Pine Mountain, GA, April 15-19, 2002

February 12, 2002

This work was performed under the auspices of the United States Department of Energy by the University of California, Lawrence Livermore National Laboratory under contract No. W-7405-Eng-48.

Mapping Phase Transformations in the Heat-Affected-Zone of Carbon Manganese Steel Welds using Spatially Resolved X-Ray Diffraction

John W. Elmer, Joe Wong, Thorsten Ressler and Todd A. Palmer

Abstract

Spatially Resolved X-Ray Diffraction (SRXRD) was used to investigate phase transformations that occur in the heat affected zone (HAZ) of gas tungsten arc (GTA) welds in AISI 1005 carbon-manganese steel. *In situ* SRXRD experiments performed at the Stanford Synchrotron Radiation Laboratory (SSRL) probed the phases present in the HAZ during welding, and these real-time observations of the HAZ phases were used to construct a map of the phase transformations occurring in the HAZ. This map identified 5 principal phase regions between the liquid weld pool and the unaffected base metal. Regions of annealing, recrystallization, partial transformation and complete transformation to α-Fe, γ-Fe, and δ-Fe phases were identified using SRXRD, and the experimental results were combined with a heat flow model of the weld and thermodynamic calculations to compare these results with the important phase transformation isotherms. From the resulting phase transformation map, the kinetics of phase transformations that occur under the highly non-isothermal heating and cooling cycles produced during welding of steels can be better understood and modeled.

Introduction

Solid-state phase transformations, such as grain growth, recrystallization, phase transitions, annealing, and tempering, all occur in the HAZ of steel welds. [1-4]. These transformations result in the formation of different HAZ microstructural sub-regions that are referred to as the coarse grained region, the fine grained region, and the partially transformed region of the weld [1-4]. The presence of these different regions is known in a qualitative sense. However, their exact size and location are not well understood because they are controlled by both the heating cycle of the weld and the kinetics of the phase transformations. Although the heating cycle of the weld can be modeled and/or experimentally measured, the kinetics of each of phase transformation is difficult to determine and is rarely known under actual welding conditions.

This lack of information has hindered the efforts to develop comprehensive models for the prediction of the HAZ microstructure, and thus our basic understanding of evolution [2]. For example, the prediction of weld microstructures from CCT diagrams requires many assumptions in order to deal with the non-isothermal and non-uniform cooling conditions of welds [2], particularly under the high temperature gradients produced by intense laser beam welding [5,6]. Furthermore, these diagrams represent the *cooling* but not the *heating* portions of the HAZ, and there is no generally accepted method for verifying how well these diagrams predict actual HAZ behavior.

Modeling the phase transformations that occur in the HAZ during welding requires both a good understanding of the temperature cycles that occur during welding and kinetics of the phase transformations. Numerical modeling of the weld temperatures has advanced considerably in the past few years and is now being used by weld researchers to calculate the size and shape of the fusion zone in carbon stels [7-9] and other alloys such as titanium [10]. These models provide accurate information about the transient three-dimensional temperature distribution around the weld, allowing the spatial distribution of peak temperatures, heating rates and cooling rates in the HAZ to be determined. However, without corresponding phase transformation kinetic models, microstructural evolution in the weld HAZ cannot be predicted. In this investigation we present SRXRD as a novel and unique experimental method for investigating microstructural evolution by directly mapping the phases that exist in the HAZ *during* welding. This map will provide validation to the numerical models, which are currently hindered by a lack of in-situ observations.

Materials and Experimental Procedures

AISI 1005 steel in the form of 10.8 cm diameter forged bar stock was used for all of the experiments. Chemical analysis was performed on this material yielding the following concentration (by wt. percent): 0.05 C, 0.31 Mn, 0.18 Si, 0.11 Ni, 0.10 Cr, 0.009 P, 0.008 Cu, 0.005 S, <0.005 Al, <0.005 Nb, <0.005 Mo, <0.005 Ti, <0.005 V. Cylindrical welding samples were machined from the as-received steel into 10.2 cm diameter bars measuring 12.7 cm long

Gas tungsten arc welds were made on the steel bars using a 225 A direct constant current welding power supply with electrode negative polarity. The average power was maintained

constant at 1.9 kW (110 A, 17.5 V) for all of the welds. Helium was used as the welding and shielding gas, and the welds were made with the torch inclined 30° from being perpendicular to the surface of the bar to prevent blocking of the diffracted x-rays. The steel bar was rotated below the fixed electrode at a constant speed of 0.11 rpm, which corresponded to a surface welding speed of 0.6 mm/s, and resulted in a ~9 mm wide fusion zone on the surface of the steel bar.

The SRXRD measurements were performed during welding using the 31-pole wiggler beam line, BL 10-2 [11] at SSRL with SPEAR (Stanford Positron-Electron Accumulation Ring) operating at an electron energy of 3.0 GeV and an injection current of ~100 mA. Details of the SRXRD welding experiments have been previously published [12-15] so only a brief description will be given here to point out some modifications to the technique.

A typical SRXRD run consisted of gathering 40 diffraction patterns, each spaced 250 μm apart, along a pre-determined path to span a range of 10 mm through the HAZ. A software package was developed on a personal computer using LabView software to control the position of the weld with respect to the x-ray beam, to control the bar rotational speed (welding speed), and to trigger the data acquisition system on a second computer. Each SRXRD data point was taken while the beam was at a fixed location with respect to the welding electrode, and data was collected for 10 s while the bar rotated under the torch at a constant speed. The resulting data were presented as a series of x-ray diffraction patterns along a given x-ray scan direction perpendicular to and away from the centerline of the weld. After completing a run, the weld was allowed to cool to room temperature and the weld was repositioned to a new starting location with respect to the x-ray beam prior to taking the next series of SRXRD data.

Results and Discussion

Phase Equilibria. Pure iron exists in both the body centered cubic (bcc) and face centered cubic (fcc) crystal forms [16]: α-Fe and δ-Fe are both bcc, while γ-Fe is fcc. In pure iron, α-Fe transforms to γ-Fe at 910°C, which is referred to as the A3 temperature. The γ-Fe reverts back to the bcc phase (now called δ-Fe) at 1390°C, which is referred to as the A4 temperature. The δ-Fe then remains stable up to the melting point at 1536°C. The AISI 1005 carbon manganese steel used in this investigation also goes through each of these phase transformations, but the microstructure contains an additional carbide phase at lower temperatures [16]. Cementite (Fe_3C) transforms to a mixture of α-Fe (ferrite) and γ-Fe (austenite) at 727°C, which is called the A1 temperature in Fe-C alloys. The principal phase transformation temperatures are commonly referred to as the A_C1, A_C3 and A_C4 on heating, and the A_R1, A_R3 and A_R4 on cooling.

Manganese, silicon and trace impurities present in the 1005 steel further alter the phase transformation temperatures, and these changes can be calculated from thermodynamic relationships. Thermocalc [17] was used to calculate the phase transformation temperatures for this particular AISI 1005 steel [18]. These calculations were made by considering the effects of Fe, C, Si, Mn, Ni and Cr on the liquid, ferrite, austenite, and cementite phase fields. The results of the phase-boundary temperatures, as calculated by Thermocalc for this multi-component alloy, are summarized in Table 1 and are illustrated in pseudo-binary form in Fig. 1.

Table 1 Calculated phase transformation temperatures for the AISI 1005 carbon manganese steel.

Transformation events On heating	Transformation	Temperature (°C)
cementite disappears (Ac1)	$Fe_3C \rightarrow (\alpha+\gamma)$	720
α–ferrite disappears (Ac3)	$(\alpha+\gamma) \rightarrow \gamma$	882
δ–ferrite reappears (Ac4)	$\gamma \rightarrow (\gamma+\delta)$	1432
austenite disappears	$(\gamma+\delta) \rightarrow \delta$	1462
liquid appears	$\delta \rightarrow (\delta+L)$	1506
ferrite disappears (liquidus)	$(\delta+L) \rightarrow L$	1529

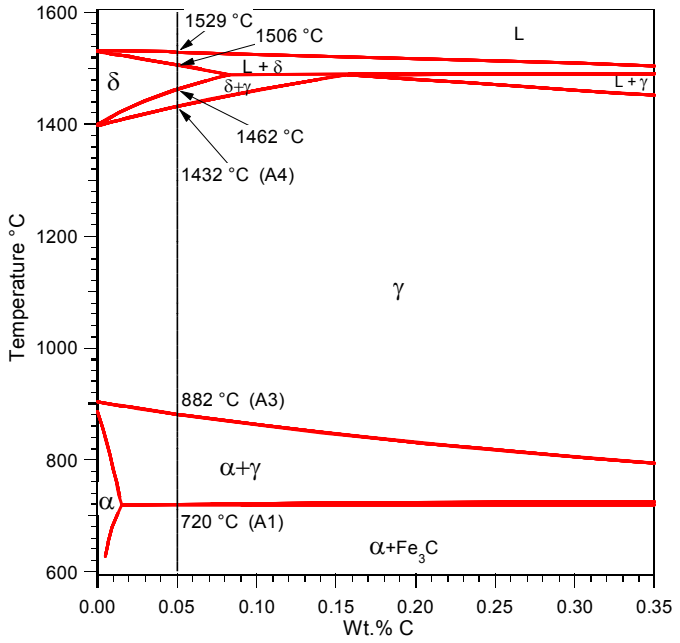

Figure 1 : Calculated pseudobinary Fe-C phase diagram for the AISI 1005 steel [18].

Base Metal and HAZ Microstructures. The microstructure of the HAZ was revealed by lightly polishing the surface of the welded steel bar and then etching in a 2% nital (nitric acid and alcohol) solution. Figure 2a shows the base metal microstructure, which is largely composed of equiaxed ferrite grains having an average diameter of 21.6 μm. Small regions of pearlite (α-Fe + Fe_3C) are present in the base metal microstructure at grain boundary edges and corners.

As welding proceeds, these new γ-Fe grains in the fine-grained region of the HAZ grow. The amount of grain growth increases rapidly as the weld fusion zone is approached, leading

to the formation of the coarse grained microstructural region of the HAZ. This coarse grained region of the HAZ is adjacent to the weld fusion zone and contains grains larger than those in the base metal. A typical microstructure from the coarse grained region of the weld is shown in Fig. 2b at a location 0.25 mm from the fusion line. This microstructure contains primarily α-Fe grains (at room temperature) that have transformed from the large prior γ-Fe grains.

The width of each microstructural subregion was measured on the metallographically prepared samples. The coarse grained region extended 0.75 mm from the fusion line, the fine grained region extended an additional 1.25 mm from the edge of the coarse grained region, and the partially transformed region extended an additional 1.0 mm from the edge of the fine grained region. The total width of the HAZ is equal to the sum of the widths of the three subregions (3.0 mm). Using the SRXRD technique, we can now follow in detail the evolution of the HAZ and various microstructural subregions contained therein as the base metal is heated and transforms along various thermal gradients during the welding process.

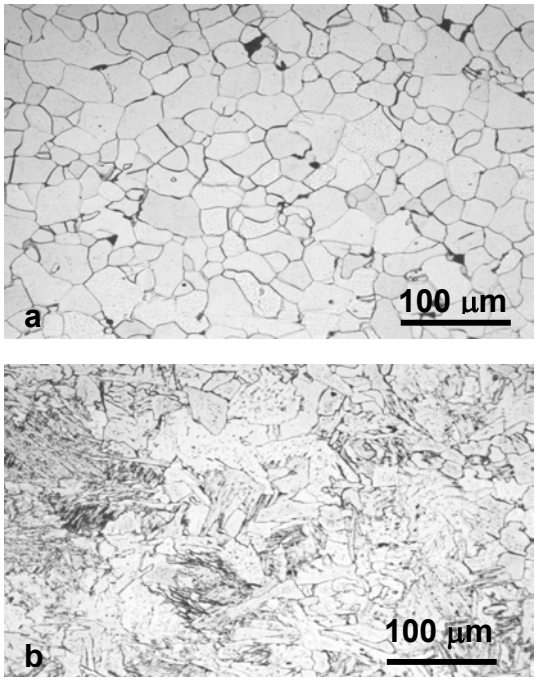

Figure 2: Optical micrographs of AISI 1005 steel fusion weld for (a) base metal, and (b) coarse grained region of the HAZ.

SRXRD Patterns. SRXRD experiments were performed *in-situ,* allowing the spatial distribution of phases present in the HAZ during welding to be determined. Diffraction patterns from the α-Fe, γ-Fe, and δ-Fe phases at specific locations within the HAZ were collected during welding. For the 1005 steel, the 2θ values of the Bragg peaks for each of the phases were calculated [19] using the lattice constants of pure iron at room temperature: 0.28665nm for the bcc phase and 0.3666nm for the fcc phase [20]. Figure 3 shows the results of these calculations at the X-ray wavelength of 0.1033 nm (12.0 keV), for non-textured crystals exhibiting no extinction effects. At this wavelength, the 2θ range of the SRXRD detector (25° to 55°) contained three ferrite peaks: the bcc (110), bcc(200), and bcc(211), and three austenite peaks: the fcc(111), fcc(200) and fcc(220).

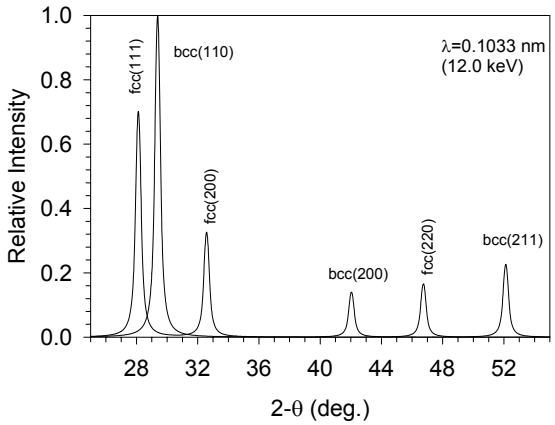

Figure 3: Calculated powder diffraction pattern for bcc-Fe and fcc-Fe at room temperature in the 2θ window of the SRXRD experiments.

Figure 4 shows a typical set of SRXRD diffraction patterns for a given weld. To gather this data, the beam was initially located in the liquid weld pool at a position 1 mm ahead of the electrode (x=-1.0) and 2 mm to the side of the electrode (y=2.0). The coordinate system used to represent the location of the x-ray beam with respect to the weld is shown in the schematic drawing that is inset in Fig. 4a. This starting position placed the beam initially in the liquid weld pool, which yielded no Bragg peaks (characteristic of the liquid state) during the first 6 frames of this sequence. As the weld jogged to new positions, the X-ray beam passed through the liquid and reached the liquid/solid interface at frame number 7 where the first diffraction peaks were observed. From this point on, Bragg peaks appeared at all HAZ locations, showing the presence of the δ-Fe, γ-Fe and α-Fe phases. These phase ratio between these phases changes across the HAZ, indicating the phase transformations that are occurring during welding.

In Fig. 4b the same data is presented as an intensity plot in two dimensions, where the lighter shades indicate higher x-ray diffraction intensity. Close attention is paid only to the low 2θ peaks. The diffraction peaks for a given phase shift to higher 2θ positions at further distances from the weld pool due the decrease in lattice parameter with decreasing temperature. This effect clearly shows the high and low temperature bcc phases in the HAZ, where the δ-Fe ferrite phase appears at a much lower 2θ peak position than the α-Fe ferrite phase.

A close examination of these figures shows that as the beam passes into the HAZ, the first two frames that exhibit diffraction peaks (7,8) show the presence of δ-Fe. In both cases the δ-Fe coexisted with a small amount of γ-Fe. In the next 5 frames (9-13) only the γ-Fe diffraction peaks were observed, showing that this portion of the HAZ had been completely austenitized by the weld thermal cycle. In the next 6 frames (14-19) both γ-Fe and α-Fe diffraction peaks were observed,

indicating the region of the HAZ where the partial transformation of α-Fe to γ-Fe had occurred. The remaining 17 frames (20-37) contained diffraction patterns only from α-Fe that was undergoing annealing and/or recrystallization. The maximum width of this HAZ is 3.25 mm as determined from the furthest SRXRD observation of the fcc phase from the fusion line. This width corresponds very well with the metallographic observations on the top surface of the weld, which showed that the outside edge of the partially transformed region of the HAZ extended 3.0 mm from the fusion line.

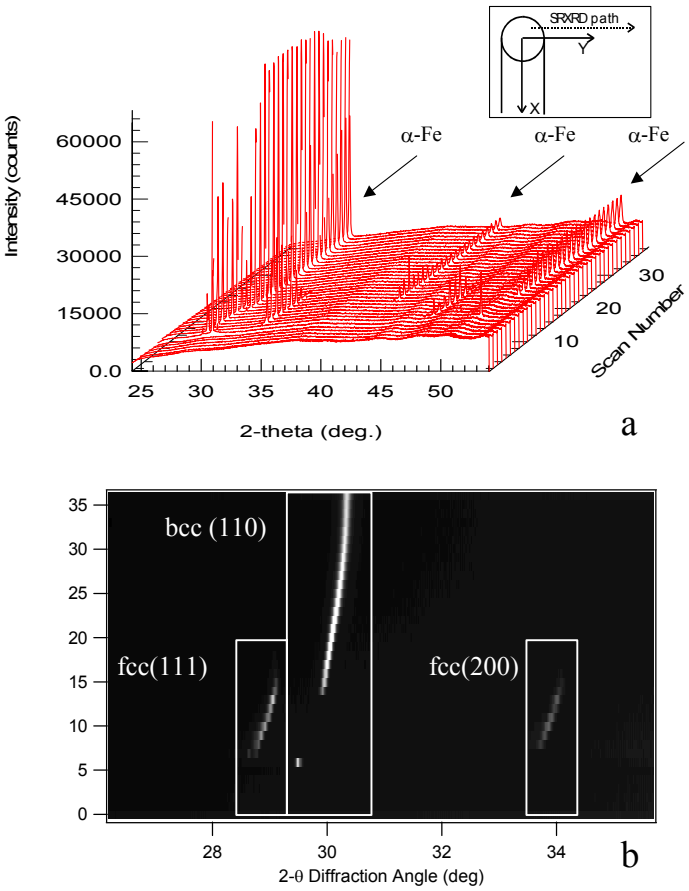

Figure 4 a) 3-d representation of a complete SRXRD scan. Thirty-seven diffraction patterns are shown starting in the liquid and moving across the weld HAZ in 0.25 mm steps in the y direction away from the weld centerline. b) The same data as in (a) but zoomed in on the lower 2θ peaks and viewed as an intensity plot where the lighter shades indicate higher diffracted peak intensity. Note peak shift to higher 2θ positions at further distances from the weld centerline for a given phase due to the thermal effect on the lattice parameter.

Spatially Resolved X-Ray Diffraction Mapping. The sequential x-ray diffraction line scans made perpendicular to the weld centerline, such as those presented in Fig. 4, were analyzed to determine both the spatial distribution of the different phases [21] and the relative fractions of each phase [22]. Each scan covered a distance of approximately 10 mm to span the width of the HAZ and contained 37 SRXRD patterns. A total of 21 individual line scans were made with the first scan at a location 6 mm ahead of the weld and the last scan at a location 17 mm behind the weld.

The completed phase identification map is shown in Fig. 5. The coexistence of γ-Fe with α-Fe, or γ-Fe with δ-Fe, was identified at numerous SRXRD locations as evidenced by simultaneous recording of the fcc and bcc diffraction patterns. These regions indicate either a phase is in the process of transforming or that two phases are coexisting in a two-phase region of the HAZ, and represents a transition region between the ferrite and austenite phases.

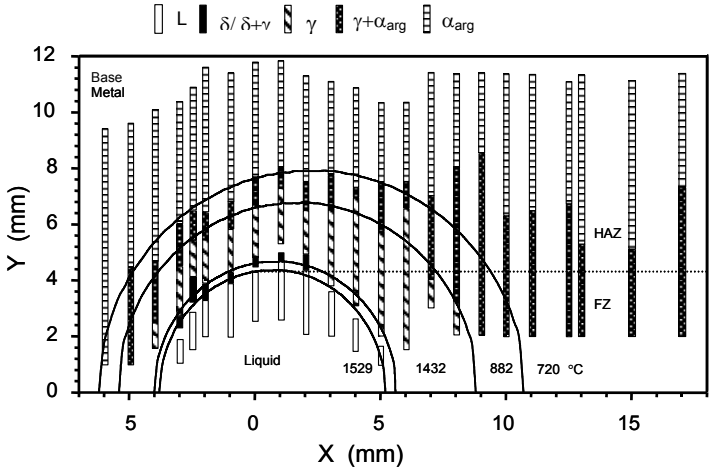

Figure 5: SRXRD phase identification map showing the locations of the α-Fe, γ-Fe, δ-Fe and liquid phases present in the AISI 1005 steel weld. The horizontal dotted line, y=4.4 mm, marks the average experimental fusion line.

Superimposed on Fig. 5 are four different weld isothermal boundaries calculated using an analytical heat flow model [21]. The calculated isotherm at 1529°C represents the liquid weld pool boundary, which extends 4.4 mm from the weld centerline. The γ/(γ+δ) boundary is represented by the 1432°C isotherm, the γ/(γ+α) boundary is represented by the 882°C isotherm, and the Fe_3C/(α+γ) eutectoid is represented by the 720°C isotherm. These calculated boundaries represent the locations where phase transformations would occur under equilibrium conditions. However, since the kinetics of the phase transformations require a finite time to take place, the location where the phase transformation is finally completed is displaced behind the calculated isotherms

The SRXRD diffraction patterns used to construct Fig. 5 contain additional information about the phase transformations in the HAZ. For example, the Bragg peaks were analyzed using peak area based methods to determine the relative fractions of α and γ in the regions of the HAZ undergoing the α→γ→α phase transformations [22]. This allowed the relative fractions of ferrite and austenite to be determined at each HAZ location. The resulting phase fraction map is presented in Fig. 6, where the gradient is shading corresponds to the gradient in the volume fraction of the austenite phase. In this map, the isotherms are now calculated using a coupled thermo-fluids model [23], which gives a more accurate prediction of the HAZ temperatures than the analytical model used in previous work [21].

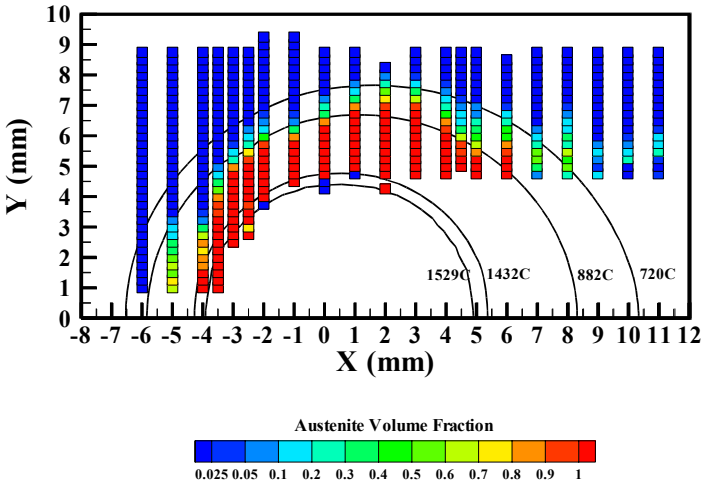

Figure 6: SRXRD semi-quantitative map showing the volume fraction austenite in the weld HAZ. Lighter shades correspond to higher volume fraction of austenite.

HAZ Phase Transformation Regions on Heating. Before the transformation to austenite begins, the α-Fe undergoes annealing, recrystallization and/or grain growth. This region extends from the A1 isotherm out to the base metal, and is characterized by SRXRD patterns that show only the bcc diffraction peaks, as indicated by the regions shaded with horizontal stripes in Fig. 5. In this region, the diffraction patterns gradually evolve from those of the base metal to those of the annealed and recrystallized microstructure [21].

These diffraction peaks from the unaffected base metal are broad due to a combination cold work [24] that results from surface machining of the steel bar, and from geometric effects from diffraction taking place over a finite distance on the curved surface of the sample bar [14]. During the heating cycle of the weld, α-Fe first begins to anneal, which has the effect of creating larger and more perfect diffraction domains than those of the base metal. This causes the diffraction peaks to reduce in width [14,24].

As α-Fe experiences more thermal exposure and higher welding temperatures, the α-Fe grains begin to recrystallize and yield very narrow diffraction. The recrystallized ferrite grains are small and nearly strain free, yielding very narrow diffraction peaks. These fine ferrite grains diffract to slightly different locations on the position sensitive x-ray detector, resulting in a tight grouping of individual spikes. These effects are similar to recrystallization observed in titanium welds using SRXRD [12,13] and the nature of the spikes in the resultant Bragg peaks is described in more detail elsewhere [14].

The α-Fe + γ-Fe two-phase region is the next region closer to the weld fusion zone, where additional time and the higher temperature have caused α-Fe to partially transform to γ-Fe. This region, shown by the shaded dots in Figure 5, is moderately large because it exists over a 162°C temperature range between the A1 and A3 as illustrated in Fig. 1. In the α-Fe + γ-Fe two-phase region of the weld, α-Fe and γ-Fe coexist in different volume fractions with the amount of γ-Fe increasing as the γ/(γ+α) boundary is approached, as shown in Fig. 6. Behind the weld, the region(s) of the HAZ that transformed partially or completely to γ-Fe during weld heating, transform back to α-Fe.

The single-phase γ-Fe region is the next region closer to the weld fusion zone, where the time/temperature cycle has been sufficient to completely transform α-Fe to γ-Fe. The single-phase γ-Fe exists over a 550°C temperature range between the A_C3 and A_C4 temperatures as illustrated in Fig. 1. This wide temperature range results in an HAZ region for the γ-Fe phase which can extend more than 1.5 mm in width at its maximum point as indicated by the calculated isotherms. The regions shaded on the diagonal in Fig. 5, show where SRXRD observed the single phase γ-Fe region, and indicate that this region first appears at a location about 4 mm ahead of the welding electrode. As the steel continues to be heated while passing beneath the arc, the γ-Fe region widens to about 1.5 mm past the fusion line as the transformation from α-Fe to γ-Fe occurs.

The δ-Fe region is the closest region to the weld fusion zone, and the SRXRD measurements where the δ-Fe phase was observed are highlighted as the solid black regions in Fig. 5. The δ-Fe phase was observed only within 0.5 mm of the liquid weld pool, and primarily on the leading edge of the weld pool. The observations of δ-Fe on the leading edge of the weld pool are significant in that the presence of δ-Fe at the liquid/solid interface provides an epitaxial template for the liquid-to-solid transformation (solidification) to δ-Fe. In the HAZ, the δ-Fe that forms on heating transforms completely to γ-Fe just past the location where the weld pool is at its maximum width.

HAZ Phase Transformation Regions on Cooling. There are two different phase transformations that occur in the HAZ during cooling. The first is the high temperature transformation of δ-Fe to γ-Fe. The SRXRD measurements show that this transformation does indeed take place close to the weld pool and goes to completion over a short distance. No δ-Fe is observed beyond 2 mm behind the weld pool as indicated in Figs. 5 and 6. The second transformation is the γ-Fe to α-Fe transformation, which occurs further away from the weld pool where the HAZ has cooled below the A_R3 temperature (882°C). This transformation is largely responsible for the microstructures that are present at room temperature since no other transformations occur after the back-transformed ferrite is formed.

The γ-Fe that transforms back to α-Fe may have three different origins within the HAZ: 1) γ-Fe that transformed from δ-Fe, 2) single-phase γ-Fe that completely transformed from α-Fe, or 3) γ-Fe that partially transformed from α-Fe. The α-Fe that back transforms from these different phase regions of the HAZ (delta ferrite, single-phase austenite, partially transformed austenite) create different microstructures after the weld has cooled to room temperature. These microstructures correspond largely to the coarse grained, fine-grained and partially transformed regions of the HAZ. These differences are the result of different nucleation and growth conditions for the γ-Fe to α-Fe transformation.

The back transformed portion of the HAZ contains α-Fe + γ-Fe, where γ-Fe was observed coexisting with α-Fe. This

region of the weld begins slightly behind the A_R3 isotherm (882ºC), where the α-Fe first nucleates and/or grows from γ-Fe. Figure 6 shows that as the transformation to α-Fe continues, the phase fraction of α-Fe increases to the point where only small γ-Fe peaks are seen coexisting with the α-Fe peaks directly behind the weld.

Conclusions

1. SRXRD was successfully used to identify and map the phases occurring in the HAZ of gas tungsten arc welds in AISI 1005 steel. These measurements constitute the first *in-situ* and direct experimental investigations of phase transformations in steel welds, and the information contained within the HAZ phase map can be used to calculate phase transformation rates under true *non-isothermal* welding conditions.
2. The SRXRD results were able to be further analyzed by Bragg peak area analysis techniques to determine the relative fractions of ferrite and austenite in the weld HAZ during welding. These results were used to determine the α and γ phase fractions in the regions of the HAZ undergoing α→γ and γ→α transformations.
3. Five principal microstructural regions were observed with SRXRD in the HAZ : (1) α-ferrite which is undergoing annealing, recrystallization and/or grain growth at subcritical temperatures, (2) partially transformed α-ferrite coexisting with γ-austenite at intercritical temperatures, (3) single phase γ-austenite at austenitizing temperatures, (4) δ-ferrite at temperatures near the liquidus temperature, and (5) back transformed α-ferrite.
4. The high temperature δ ferrite phase was observed at locations primarily within 0.5 mm of the liquid weld pool. The δ-Fe phase was observed to back transform quickly and completely to γ-Fe just past the location where the weld pool was at its maximum width. The presence of δ-Fe adjacent to the liquid weld pool provides the opportunity for epitaxial growth of the bcc phase from the liquid weld pool during solidification.

Acknowledgments

This work was performed under the auspices of the U. S. Department of Energy, by the U.C, Lawrence Livermore National Laboratory, under Contract No. W-7405-ENG-48. T. R. thanks the Alexander von Humboldt Foundation for a Feodor Lynen research fellowship. The synchrotron experiments were carried out at SSRL supported by DOE, the Division of Chemical Science. The authors would like to express their gratitude to Dr. Suresh Babu for assisting with the data analysis, Mr. A. T. Teruya of LLNL for writing the LabView software to control the welding experiments, and Mr. B. Kershaw of LLNL for performing optical metallography.

References

1. Ø. Grong, *Metallurgical Modelling of Welding*, The Institute of Materials, London, Chapter 1, (1994)
2. K. Easterling, *Introduction to the Physical Metallurgy of Welding*, Butterworths and Co., Chapter 3, (1983)
3. M. F. Ashby and K. E. Easterling, *Acta Metall*., V30, p. 1969, (1982)
4. J. C. Ion, K. E. Easterling, and M. F. Ashby, *Acta Metall*., V32, p. 1949, (1984)
5. M. Frewin, D. Dunne, and A. Scott, *Science and Technology of Welding and Joining*, V3(3), 9. 145, (1998)
6. M. F. Ashby and K. E. Easterling, *Acta Metall*., V32, p. 1935, (1984)
7. Z. Yang and T. DebRoy, *Science and Technology of Welding and Joining*, Vol 2(2), p. 1, (1997)
8. K. Mundra, T. DebRoy, S. S. Babu and S. A. David, *Welding Journal*, 76(4), p. 163-s, (1997)
9. Z. Yang and T. DebRoy, *Metall. Mater. Trans. B, 30B,* pp. 483-493, (1999)
10. Z. Yang, J. W. Elmer, Joe Wong, and T. DebRoy, *Welding Journal*, 79(4), p. 97s-112s, (2000)
11. V. Karpenko, J.H. Kinney, S. Kulkarni, K. Neufeld, C. Poppe, K.G. Tirsell, Joe Wong, J. Cerino, T. Troxel, J. Yang, E. Hoyer, M. Green, D. Humpries, S. Marks, and D. Plate: *Rev. Sci. Instrum.*, 60, p.1451, (1989)
12. J. W. Elmer, Joe Wong, M. Fröba, P. A. Waide and E. M. Larson, *Metall. Mater. Trans. A,* 27A(3), p. 775, (1996)
13. J. W. Elmer, Joe Wong and Thorsten Ressler, *Metall. Mater. Trans. A*, 29A(11), p. 2761, (1998)
14. Thorsten Ressler, Joe Wong and J. W. Elmer, *J. Phys. Chem. B*, 102(52), p. 10724, (1998)
15. Joe Wong, M. Fröba, J. W. Elmer, and P. A. Waide, *J. Mat. Sc.*, 32, p. 1493, (1997)
16. R. W. K. Honeycomb, *Steels- Microstructure and Properties*, American Society of Metals, (1982)
17. B. Sundman, B. Jansson and J. Andersson: Calphad-Computer Coupling of Phase Diagrams and Thermochemistry, V 9(2), p.153, (1985)
18. Calculations performed by Dr. Suresh Babu of Oak Ridge National Laboratory, March, (2000)
19. *PowderCell, v. 1.0,* W. Kraus and G. Nolze, Federal Institute for Materials Research and Testing, Rudower Chaussee 5, 12489 Berlin, Germany. A free version may be obtained by request to gert.nolze@Bam.de.
20. Metals Handbook, Ninth Edition, Vol. 3, *ASM International*, (1979).
21. J. W. Elmer, Joe Wong and Thorsten Ressler : *Metall. and Mater. Trans. A*, 32A (5), pp. 1175-1187, (2001)
22. Unpublished research, Dr. Todd Palmer and Brandon Wood, Lawrence Livermore National Laboratory, 2001.
23. W. Zhang, J. W. Elmer, and T. DebRoy, "Modeling and Real Time Mapping of Phases during GTA Welding of 1005 Steel," in press, *Materials Science and Engineering A*, February, 2001.
24. B. D. Cullity, *Elements of X-Ray Diffraction*, Addison Wesley, p. 263, (1956).